Establishing a West African chrono-cultural framework: First luminescence dating of sedimentary formations from the Falémé Valley, Eastern Senegal

Brice Lebrun, Chantal Tribolo, Benoît Chevrier, Michel Rasse, Laurent Lespez, Alice Leplongeon, Irka Hajdas, Abdoulaye Camara, Norbert Mercier, Éric Huysecom

Establishing a West African chrono-cultural framework: First luminescence dating of sedimentary formations from the Falémé Valley, Eastern Senegal

Brice Lebrun, Chantal Tribolo, Benoît Chevrier, Michel Rasse, Laurent Lespez, Alice Leplongeon, Irka Hajdas, Abdoulaye Camara, Norbert Mercier, Éric Huysecom

Journal of Archaeological Science: Reports 7 (2016) 379–388

Establishing a West African chrono-cultural framework: First luminescence dating of sedimentary formations from the Falémé Valley, Eastern Senegal

Brice Lebrun [a,*], Chantal Tribolo [a], Benoît Chevrier [b], Michel Rasse [c], Laurent Lespez [d], Alice Leplongeon [e,h], Irka Hajdas [f], Abdoulaye Camara [g], Norbert Mercier [a], Éric Huysecom [b]

[a] *IRAMAT-CRP2A, UMR 5060, CNRS, University of Bordeaux Montaigne, Pessac, France*
[b] *APA, Department of Genetic and Evolution, University of Geneva, Switzerland*
[c] *Archéorient, UMR 5133, MSH Maison de l'Orient et de la Mediterranée, University of Lyon 2, France*
[d] *Laboratoire de Géographie physique (LGP), UMR 8591, CNRS, University of Paris-Est Créteil, France*
[e] *Museum national d'Histoire naturelle, UMR CNRS 7194, Departement of prehistory, Paris, France*
[f] *Laboratory of Ion Beam Physics, Zurich, Switzerland*
[g] *Institut Fondamental d'Afrique Noire (IFAN), Cheikh Anta Diop University, Dakar, Senegal*
[h] *McDonald Institute for Archaeological Research, University of Cambridge, UK*

Keywords:
Palaeolithic West Africa Falémé Valley OSL Luminescence dating Single grain Pleistocene

a b s t r a c t

Recent studies have shown that the Falémé Valley, located in eastern Senegal, is a major component in the com- prehension of the West African Palaeolithic period. Several of the sites discovered in this region show a wide va- riety of lithic productions attributed to the Early, Middle and Later Stone Age.

Optically stimulated luminescence dating of 16 samples coming from five sites produces evidence of archaeolog- ical records from at least Marine Isotope Stage 5, highlighting an ancient human presence. The dates also indicate nearly continuous sedimentary deposits over the entire upper Pleistocene. In particular, at least one archaeolog- ical level is positioned within Marine Isotope Stage 2, which is poorly documented in West Africa. Thus interest- ingly, the Falémé sequence completes the sequence of Ounjougou in Mali, which was considered up to now as the unique key element for the definition of the chrono-cultural framework of this region.

1. Introduction

Until recently, West Africa was excluded from the general discussion and models concerning the dynamics of Palaeolithic populations, both during the Middle and Upper Pleistocene (e.g.: Mcbrearty and Brooks, 2000; Garcea, 2012; Lombard, 2012; Chevrier et al., submitted). A rea- son for this is the scarcity of palaeo-anthropological data and the small number of available dated sequences. Within the considered area, Oldowan-like or Acheulean-like industries could be identified but not yet directly dated (e.g.: Sansandé, Camara and Duboscq, 1984, 1990; Ounjougou site complex, Soriano et al., 2010a, 2010b). The rele- vant artifacts are rarely found in complete (reasonable) stratigraphic context, leading to *terminus ante quem* at best. The only exceptions might be two partially burned trihedral bifaces from Tilemsi valley (Mali) dated by thermoluminescence (TL) to 282 ± 56 ka (Diop, 1980) and the Oldowan-like assemblage of Kokolo 2 in Ounjougou, dated by Optically Stimulated Luminescence methods (OSL) to an unex- pectedly recent time period, within Marine Isotope Stage (MIS) 4. This last result highlighted the risk of relying only on typological information for establishing a chrono-cultural framework.

For the assemblages attributed to the Middle Stone Age (MSA) period, few isolated sites provided numeric chronological data. Birimi in Ghana has been dated by OSL to 41 ka and yielded discoid and Levallois cores (Hawkins et al., 1996; Casey et al., 1997; Quickert et al., 2003). Bilma in Niger, where Levallois cores were discovered, has been dated by radiocar- bon to more than 33 ka BP uncal (Maley et al., 1971). The study of the Ounjougou complex and the nearby site of Songona, both in Mali, signif- icantly extended the chronological and technological data set for this timeframe. Over 20 MSA occurrences were recognized and dated by OSL, covering MIS 4 and 3 (Huysecom, 2002; Huysecom et al., 2007; Soriano et al., 2010a, 2010b; Rasse et al., 2012; Tribolo et al., 2015). In ad- dition to Levallois and discoid debitages, bifacial foliates or heavy scrapers shaping, bipolar on anvil flaking, and laminar productions were also iden- tified, showing a high variability and suggesting cultural instability and/or high mobility of prehistoric societies during this period.

* Corresponding author.
E-mail address: brice.lebrun@u-bordeaux-montaigne.fr (B. Lebrun).

At Ounjougou, MIS 2 is marked by a sedimentological and thus cul- tural gap. For now, only three lines of evidences for human occupation are attested in West Africa during this MIS. All are close to the Gulf of Guinea: Shum Laka in northwest Cameroon, from 30 ka to 10 ka BP uncal, Bingerville on the Ivory Coast (ca. 13 ka BP uncal) and Iwo Eleru in Nigeria (ca. 11 ka BP uncal) (Chenorkian, 1983; Shaw and Daniels, 1984; Cornelissen, 1996, 2003). The chronological attribution of Mayo Louti in Cameroon to MIS 2 (more than 15 ka BP uncal) is less secure (Marliac, 1973; Marliac and Gavaud, 1975). Except for Mayo Louti (which displays a MSA-like assemblage), microliths and backed pieces are the frequent artifacts in these sites.

Note that, despite a particularly important number of palaeolithic sites studied in Senegal (Huysecom, 1987; Huysecom et al., 2013), none appears in the above mentioned list of dated sites, since previous studies used only relative dating techniques (e.g. Camara and Duboscq, 1984). Since 2012, the *Human Population and Paleoenvironment in Africa* project (PHPA) has focused on the Falémé Valley, eastern Senegal (Fig. 1), which has proved to be important be- cause of the richness of its archaeological record (Chevrier et al., in press), and because of its great chrono-stratigraphic potential. In this paper, we present the first OSL chronological data for the Falémé Valley sequences in which five archaeological sites were recognized and exca- vated between 2013 and 2015 by the PHPA team.

2. Regional settings

2.1. Geomorphological context

In the Falémé Valley, several levels of river terraces have long been known (Michel, 1973; Camara and Duboscq, 1984). Camara and Duboscq (1984) have distinguished three main alluvial formations. A chronological framework was proposed thanks to the correlation be- tween geomorphological observations and oxygen-isotope records (marine cores off the Mauritania and Senegal coasts; Camara and Duboscq, 1987), covering MIS 10 to the Holocene. The sedimentation of alluvial, colluvial and aeolian formations was assumed to be almost continuous, even though no direct numerical data was produced at that time. Therefore, while the Falémé river seemed to present the op- portunity to track the environmental and archaeological changes at the end of the Pleistocene, the lack of systematic geomorphological in- vestigations of the quaternary formations in order to accurately describe their geometry on the one hand, and the lack of absolute dates on the other hand, made the chrono-stratigraphy hypothetical. The investiga- tions performed between Alinguel in the South and Missira in the North, during the 2011 to 2015 fieldworks, offered the opportunity to reconstruct the organization of the main stratigraphic units for the Late Quaternary period and to revise the results of the previous re- search. Fig. 2 shows the entire stratigraphic sequence. All formations were superimposed in order to illustrate the potential of this area, but the longitudinal integration of each one relatively to the stratigraphic units is obviously more complex. On a recurring basis, we note an alter- nation of fine deposits, probably of aeolian origin but reworked due to colluvial and fluvial processes (units "U": U_B, U_J, U_S, U_C and U_G), and coarser deposits, generally channelized, rich in coarse gravels, fine gravels and sands. They comprise limestone pisiform concretions reworked from the nearby ferruginous indurated hard crust (units "C": C_{AG}, C_{BJ}, C_{JS}, C_{SC} and C_{Sup}). This alternation testifies to rapid succes- sion of periods during which the sedimentation was mainly linked to flood phenomena, leading to a reconfiguration of the fine particles from the watershed, and sudden and short periods of events incising an- terior formations.

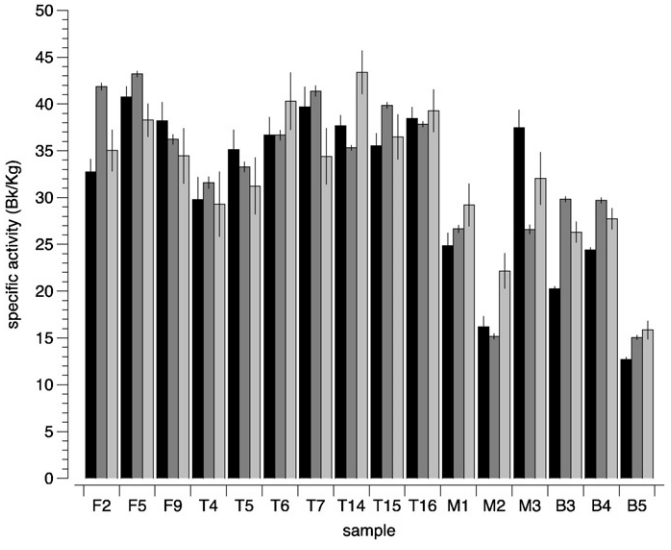

Fig. 1. Location of the Falémé Valley in West Africa and archaeological sites discussed here.

2.2. Archaeological context

Over 106 archaeological occurrences have been (re)discovered up to now in the Falémé Valley. This paper focuses on five major sites located between Alinguel and Missira: Fatandi V, Toumboura I and III, southern ravine of Missira ("Ravin de Missira") and the banks of the river near Alinguel ("Berges d'Alinguel"). A rapid overview of each site is given here while extensive information can be found in Chevrier et al., in press. The location of these sites is displayed on Fig. 1.

"Berge d'Alinguel" has yielded many rolled pieces on the surface and several were found in stratigraphy; all of them present an archaic look (pebble-tools, handaxes, large flakes, etc.) and could be characteristic of the Early Stone Age (unit C_{AG}). "Ravin de Missira" yielded a rolled and broken bifacial point in secondary position, which could be charac- teristic of the MSA. This artifact was found in a coarse formation be- tween fine sediment of alluvial formations inserted into the main sequence in the form of a lateral valley. At Toumboura III, lithic artifacts (shaping flakes, bifacial pieces) are characteristic of the MSA and were found in one unique archaeological layer attributed to the U_J unit. At Fatandi V, numerous lithic artifact concentrations were recognized on the surface and one single archaeological layer is present in stratigra- phy. This layer has yielded artifacts linked to multiple modes of produc- tion and varied volumetric conceptions (in particular bladelet debitage on wide surface), which aim is mainly wide bladelets. Two large seg- ments made in a different raw material were also collected. The correla- tion of Fatandi V deposits to the general stratigraphic scheme is not yet clear though an early age is expected. Toumboura I presents a high number of lithic material at the ground surface. A single archaeological layer takes place inside the Grey Unit (U_G). The material is very fresh and characteristic of a primary position occupation. The majority of the artifacts is composed of small flakes and bladelets, obtained by debitage of small silexite blocks without (or with little) preparation. These products were used as blanks for microlithic backed segments and points. Medium-sized flakes of siliceous rock and sandstone were also collected. This short overview shows that the lithic assemblages display a great technological variability and absolute dating is crucial to contextualize and help understanding it.

3. Sampling

We present here the results for 16 samples coming from five sites mentioned in Section 2.2 and Fig. 1. Theses samples have been collected during three field trips in 2013, 2014 and 2015, in close collaboration with the archaeologists, geologists and geomorphologists of the PHPA project.

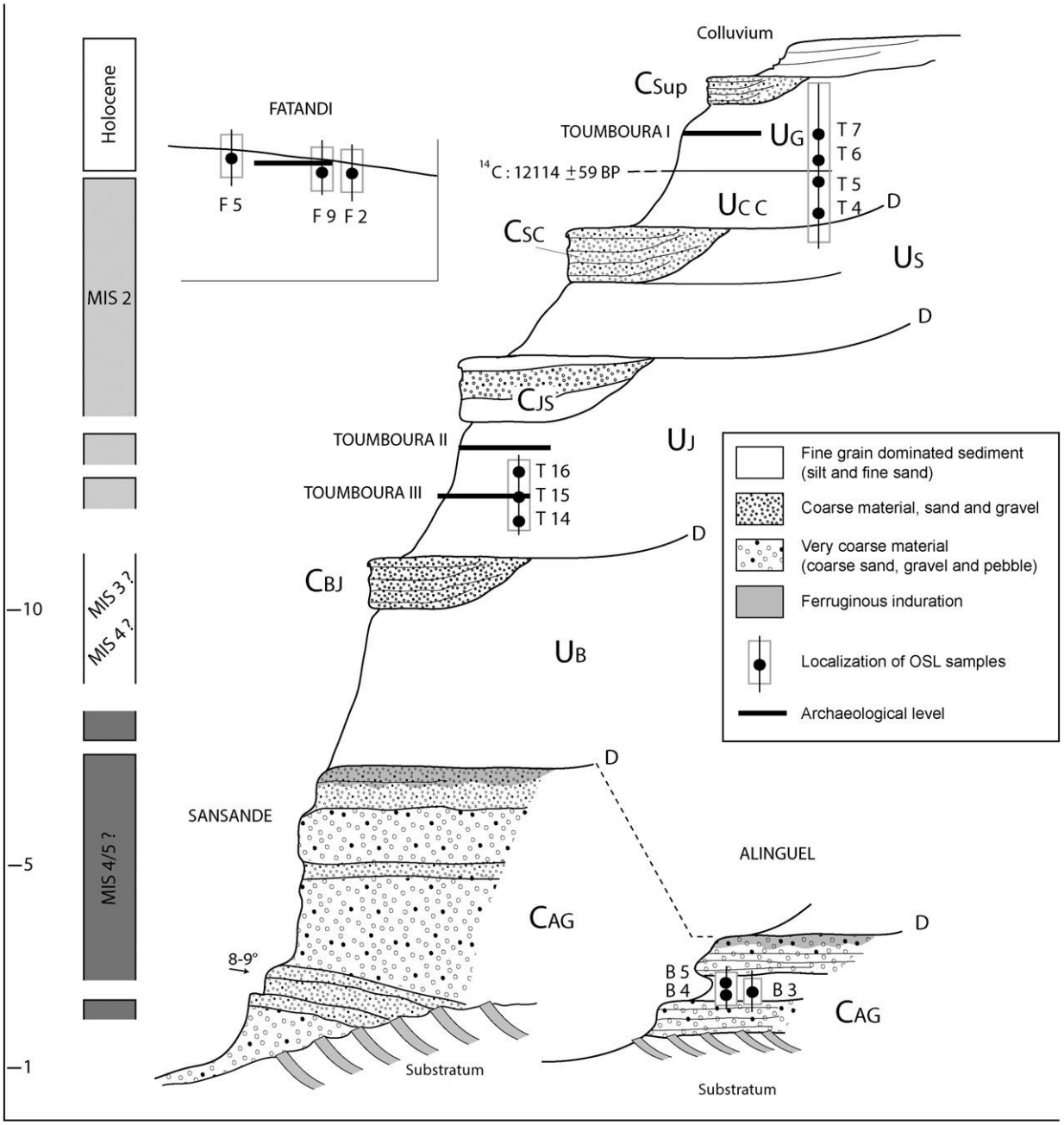

Fig. 2. Synthetic stratigraphic sequence of the Falémé Valley and location of OSL samples. Samples M1, M2 and M3 are not represented here since they are located in lateral formations inserted in the represented sequence. For the same reason, the insertion of Fatandi and Alinguel into the main sequence is still under investigation and is therefore represented here beside the main stratigraphic sequence.

Three samples (B3, B4 and B5) were collected at "Berges d'Alinguel" in a fine deposit level located above a coarse deposit where the artifacts were found (U_{AG}), at the base of the main sequence. In the "Ravin de Missira", samples M1, M2 and M3 were collected near the broken bifa- cial point into fine to sandy sediment located between coarse deposits. The broken bifacial point is located between sample M1 and M2. At this stage, more precise identification of the stratigraphic position of the bifacial point and these three samples are still under investigation. Samples T14, T15 and T16 were taken from Toumboura III and were re- spectively collected at the bottom, in the middle and at the top of the archaeological layer which is located inside the U_J formation. Four OSL samples were taken at Toumboura I: T4 and T5 were collected in U_{CC} and T6 and T7 in U_G. Sample T7 corresponds to the archaeological level. It can be noted that an age of 12,114 ± 59 BP uncal (ETH-55080) or 12,008 ± 176 2σ cal BCE (Reimer et al., 2013) is given by radiocarbon dating for a charcoal located between T5 and T6, 60 cm under the archaeological layer (Chevrier et al., in press). At Fatandi V, while samples F2 and F9 are located 20 cm under two lithic concentrations, F5 was taken in a layer located in the upper part of this site. A synthetic overview of the correspondence between the samples and the strati- graphic units is given in Table 3 and in Fig. 2.

In the field, sampling was systematically performed at night by sur- face scratching. First, at least 1 cm of sediment was discarded in order to remove grains that could have been exposed to daylight. Then, the sed- iment sample intended for luminescence measurements was collected into light-tight bags. In the hole left by the sampling, a 7 cm diameter hole (30 cm long) was mechanically drilled and the gamma dose rate determined using a portable gamma spectrometer.

4. OSL dating

4.1. Dose rate determination

The U, Th and K contents of the sediment samples were determined by high resolution gamma spectrometry (broad energy germanium de- tector). Prior to analysis, about 20 g of each sample was finely crushed and sealed in a plastic box for 30 days in order to ensure that the equi- librium between the ^{226}Ra and post-radon emitters of the uranium se- ries was reached. Fig. 3 shows the activities of the "beginning" (^{238}U deduced from the activities of ^{234}Th, ^{234m}Pa and ^{235}U), "middle" (^{226}Ra deduced from the measured activity of ^{214}Pb and ^{214}Bi) and "tail" (^{210}Pb) which vary from ca. 13 to 62 Bq/kg, depending on the sample. These measurements do not indicate any significant disequilibrium but this observation is actually poorly informative since one has no ac- cess to the mean ^{226}Ra activity over the burial time of the dated grains in the sediments.

The water content in the sediments, averaged over the time of burial of the grains, has to be estimated since water attenuates the radiations and consequently lowers the dose received by the quartz grains. Follow- ing Nelson and Rittenour (2015), the water saturation level of each sed- iment sample was computed using its particle size distribution (Table 1). The water saturation levels range between 20 and 25%. For each sediment, the past mean water content has been arbitrarily set to 50 ± 15% of its saturation level as possible changes of this value over time are unknown.

Dose rate conversion factors of Guérin et al. (2011), and attenuation factors of Guérin and Mercier (2011), were used for calculation and the derived beta dose rates are presented in Table 1. These values range from 0.53 ± 0.01 to 2.15 ± 0.03 Gy/ka and represent approximately half of the total dose rate.

Field gamma spectra have been acquired with a Canberra Inspector 1000 portable spectrometer (LaBr probe) and were analyzed according to the energy threshold technique (Mercier and Falguères, 2007; Guérin and Mercier, 2011). The gamma dose rates, being accounted for water content of the sediment at the time of counting, range from 0.42 ± 0.01 to 0.93 ± 0.02 Gy/ka (statistical uncertainties) and contribute to ca. 40% of the total dose rate.

Cosmic dose rates were computed according to Prescott and Hutton (1994), taking into account the GPS coordinates, the altitude of the sites, and the estimated sediment density above the samples. Since the burial depths of the samples have likely varied over time, an uncertainty on the cosmic dose rate of 10% was considered. However, it should be noted that the cosmic contribution to the total dose rate is only ca. 10%, with values ranging from 0.11 ± 0.01 to 0.19 ± 0.02 Gy/ka. Consid- ering all the dose rate contributions, the total dose rates range from 1.06 ± 0.01 to 3.12 ± 0.02 Gy/ka (Table 1) (statistical uncertainties). For age calculation, systematic uncertainties were applied as follows: 10% for uranium, thorium and potassium contents, 10% for cosmic dose, 5% for in-situ gamma dosimetry.

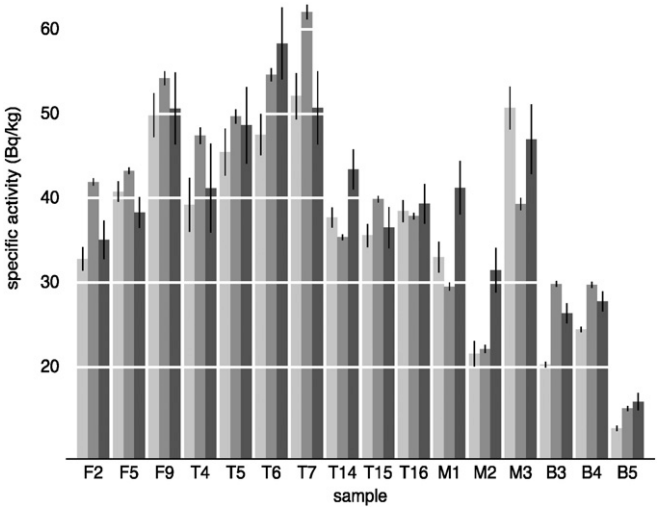

Fig. 3. Comparison between specific activities from "beginning" (^{238}U deduced from the activities of ^{234}Th, ^{234m}Pa and ^{235}U), "middle" (^{226}Ra deduced from the measured activity of ^{214}Pb and ^{214}Bi) and "tail" (^{210}Pb) radioisotopes of the uranium decay chain; respectively from left to right. Uncertainties are displayed at 1σ.

4.2. Equivalent dose determination

All the laboratory work has been conducted under subdued red- orange light. Prior to analysis, the 100–140 μm fraction of the sediment was selected by wet sieving. Carbonates and organic matter were elim- inated by successive baths (10% HCl for 60 min and 30% H_2O_2 for 48 h, respectively), each bath being followed by at least three demineralized water rinsing. Quartz grains were then isolated from feldspars and heavy minerals using sodium heteropolytungstate heavy liquids (re- spectively at densities of 2.58 and 2.72 g/cm^3). Quartz grains were etched with 40% hydrofluoric acid during 40 min with manual stirring. Rinsing with 10% HCl was then performed to eliminate potential fluori- nated compounds, followed by a final wet sieving in order to remove grains under 80 μm.

Luminescence measurements were carried out either in multi-grain or single-grain mode, respectively with a Lexsyg Smart reader (Richter et al., 2013) and a Risø TL/OSL-DA-20 reader (Duller et al., 1999; Bøtter-Jensen et al., 2000, 2003).

Prior to further analyses, depletion ratio tests (Duller, 2003) were conducted to check for the absence of feldspar grains in the quartz ex- tracts. Characterization of the luminescence signal was performed in order to assess whether any ultrafast or medium components (which are not suitable for luminescence dating) were present. Multi-grain discs were analyzed with linear modulation (LM) of the LED power (from 0 to 70 mW/cm^2 in 2000 s). The LM-OSL signals were compared with those obtained from the Risø calibration quartz (Fig. 4), and were found to be dominated by the fast component. Moreover, the first series of tests indicated that the quartz grains were very bright, since in some cases the stimulation power commonly used (90 mW/cm^2) had to be lowered to 25 mW/cm^2 due to photo-multiplier saturation issues.

A single aliquot and regenerative dose protocol (Murray and Wintle, 2000; Wintle and Murray, 2006) was applied to all samples. Six regen- erative doses (including a zero dose and a dose given twice, at the be- ginning and at the end of the sequence) were delivered. Their values were chosen as fractions of the roughly estimated De of each sample, following the suite: 1/3, 2/3, 4/3, 6/3, 0, 1/3. For choosing the test dose value, dose recovery tests were performed with test dose values ranging from 2 to 30 Gy, but no significant impact on the dose recovery ratios was detected. Therefore, in the regenerative dose protocol, a test dose of 4.8 Gy was used in multi-grains mode and 2.8 Gy in single-grain mode. In the multi-grains mode, the stimulation lasted for 100 s but the luminescence signal was integrated on the first 0.3 s and the back- ground during 5 s starting at second 20 of stimulation (however, late in- tegration background (last 10 s) produced no significant change in the integrated signal intensity). In the single grain mode, the stimulation last for 1 s while the luminescence and background signals were inte- grated during the first 0.17 s in the first case and over the last 0.15 s for the latter. A saturating exponential function was used for the con- struction of the growth curve. Data analysis was performed with the Analyst software (Duller, 2015).

The stability of the estimated De over preheat conditions was test- ed with multi grain discs: plateau tests were performed for 11 samples by varying the preheat temperature of the regenerative doses between 160 and 300 °C, while the preheat temperature of the test dose remained constant (either 160, 200 or 220 °C, each for 0 s). Since multi-grain mode does not allow to perform grain selection based on D_0 criteria (see below), such plateau test must be considered with

Table 1
Data related to the calculation of the dose rate. W.F.: estimated water content in the sediment during burial, (mass of water/mass of dry sediment in %); W: water content (%) in the sat- urated sediment; intervals for size fraction are 0 to 3.9 (clay), 4 to 62.9 (silt) and 63 to 200 μm (sand) following Nelson and Rittenour, 2015; see Section 4.1. The grain size distribution was obtained with a Horiba LA950 laser diffraction analyzer using 2 g of sample previously treated with hydrogen peroxide and sodium hexametaphosphate for 12 h, and dispersed into water with 60 s of ultrasonification in the micro-granulometer. The Mie solution to the Maxwell equation (Mie, 1908) was used to calculate the particle size distribution from the measured scattering of light using refractive indices of 1.333 for water and 1.55–0.01 i for sediment. Doses represented here include the contribution of water. In addition to statistical errors, beta and gamma dose rates were assigned systematic errors of respectively 10 and 5% to account for detectors calibration. Cosmic dose rates were assigned a 10% uncertainty. Total dose rate uncertainties represented are global (including both systematic and statistic errors).

Site	Sample	Burial depth (cm)	Radionuclide content			Particle size distribution (%)			Water content		Annual dose rate (Gy/ka)			
			U (ppm)	Th (ppm)	K (%)	Clay	Silt	Sand	W.F.	W	Beta	Gamma	Cosmic	Total
Fatandi V	F2	30	3.39 ± 0.03	9.45 ± 0.09	0.94 ± 0.01	20	58	22	0.11 ± 0.02	0.22	1.15	0.85	0.19	2.18 ± 0.15
	F5	90	3.5 ± 0.03	10.45 ± 0.08	1.15 ± 0.01	20	71	9.0	0.12 ± 0.02	0.23	1.31	0.93	0.18	2.41 ± 0.17
	F9	54	2.93 ± 0.04	9.55 ± 0.12	1.02 ± 0.02	3.0	74	23	0.13 ± 0.02	0.25	1.14	0.85	0.18	2.18 ± 0.25
Toumboura I	T4	354	2.56 ± 0.05	9.63 ± 0.14	1.11 ± 0.03	20	53	27	0.11 ± 0.02	0.21	1.18	0.84	0.13	2.14 ± 0.29
	T5	308	2.70 ± 0.04	9.59 ± 0.12	1.06 ± 0.02	18	55	27	0.11 ± 0.02	0.22	2.15	0.83	0.13	3.12 ± 0.25
	T6	188	2.97 ± 0.04	10.03 ± 0.11	1.14 ± 0.02	20	52	28	0.11 ± 0.02	0.22	1.25	0.92	0.16	2.33 ± 0.26
	T7	165	3.35 ± 0.05	11.07 ± 0.12	1.11 ± 0.02	18	58	24	0.11 ± 0.02	0.22	1.29	0.91	0.16	2.36 ± 0.26
Toumboura III	T14	180	2.86 ± 0.02	9.67 ± 0.07	0.96 ± 0.01	14	69	17	0.12 ± 0.02	0.23	1.11	0.82	0.16	2.09 ± 0.15
	T15	145	3.22 ± 0.03	9.95 ± 0.08	0.96 ± 0.01	19	70	11	0.12 ± 0.02	0.23	1.15	0.84	0.16	2.15 ± 0.15
	T16	120	3.06 ± 0.02	10.45 ± 0.08	0.99 ± 0.01	32	57	11	0.12 ± 0.02	0.24	1.16	0.86	0.17	2.18 ± 0.16
Missira	M1	436	2.16 ± 0.03	5.00 ± 0.07	0.59 ± 0.02	3.0	42	55	0.11 ± 0.02	0.21	0.71	0.42	0.11	1.25 ± 0.17
	M2	328	1.23 ± 0.02	4.31 ± 0.06	0.48 ± 0.01	3.0	42	55	0.11 ± 0.02	0.21	0.53	0.44	0.13	1.06 ± 0.12
	M3	215	2.15 ± 0.04	9.53 ± 0.12	0.91 ± 0.02	18	63	19	0.11 ± 0.02	0.22	1.00	0.76	0.15	1.91 ± 0.23
Berges d'Alinguel	B3	60	1.64 ± 0.02	7.37 ± 0.07	0.99 ± 0.01	17	52	31	0.11 ± 0.02	0.21	0.96	0.65	0.18	1.79 ± 0.12
	B4	120	1.98 ± 0.02	7.35 ± 0.07	0.99 ± 0.01	12	63	25	0.11 ± 0.02	0.22	1.00	0.58	0.17	1.75 ± 0.12
	B5	100	1.03 ± 0.02	3.72 ± 0.06	1.39 ± 0.02	9.0	40	51	0.10 ± 0.02	0.20	1.11	0.56	0.18	1.85 ± 0.13

caution. An example of preheat plateau is given in Fig. 5. Except for ex- treme values (e.g. 160 and 300 °C), the De values do not vary signifi- cantly and a preheat temperature of 260 °C was chosen for all additional measurements done with multi-grains aliquots. The preheat temperature was either 240 or 260 °C, with a test dose cut heat at 160, 200 or 220 °C.

During inspection of the growth curves, selection criteria were ap- plied in both multi and single grain modes: a recycling ratio within 10% of unity and a recuperation ratio lower than 5%. In the single grain mode, an additional criteria based on the growth curve saturation parameter (D_0) was also used. A rough estimate of the De values indi- cated that some of our samples have high accumulated doses, up to 150 Gy. Multi-grain dose recovery tests performed for such doses show that the mean recovered dose is clearly underestimated, while these tests are satisfying for lower dose values (we considered as acceptable dose recovery ratios included in the [0.9; 1.1] interval). This might be due to the influence of a significant amount of grains for which the dose saturation level has been reached. These grains, which are unable to record the whole dose they receive, must thus be discarded. Dose recovery tests were thus conducted at the single grain level. Bleaching was performed with a Hölne uvaCUBE 400 solar simula- tor during 60 s. It was observed that, when grains with low D_0 values were included in the distribution of the recovered De values, the dose recovery ratios were significantly below 0.9 ("Berges d'Alinguel", "Ravin de Missira" and Toumboura III), consistent with the multi-grain dose recovery ratios. However, when the grains with lower D_0 values have been progressively removed, as suggested by Thomsen et al. (2016) and Guérin et al. (2015), the dose recovery ratio increases and reaches a plateau within the [0.9; 1.1] interval, as required (Fig. 6). As a consequence, this selection of grains is important for samples that

Table 2
Data related to the determination of the equivalent doses. Acquisition modes are either multi-grain (MG) or single-grain (SG); for both modes, system reproducibility (1.5% in multi-grain and 2.5% in mono-grain) has been taken into account for De calculation; N: number of grains or aliquots measured for De determination; n: number of grains or aliquots selected; OD: over- dispersion of De value (for single-grain measurement, OD values are computed once D_0 criteria is applied). The final De is estimated using the central age model (CAM) of Galbraith et al. (1999). The error on the De value corresponds to the statistical error. For age calculation, a systematic error of 4% on the De was applied in order to take into account the uncertainty of the calibration of the source.

Site	Sample	Aquisition mode	Dose recovery test					Equivalent dose					
			N	D_0 threshold value (Gy)	n	ratio	OD (%)	N	Saturated grains (%)	D_0 threshold value (Gy)	n	OD (%)	CAM De (Gy)
Fatandi V	F2	MG	5	–	5	1,02 ± 0,01	0 ± 0	51	–	–	51	22.5 ± 2.4	22.8 ± 0.8
	F5	MG	3	–	3	1.01 ± 0.02	0 ± 0	30	–	–	30	13.7 ± 1.9	19.0 ± 0.5
	F9	SG	300	None	46	1.00 ± 0.01	4 ± 2.2	2400	3	None	388	33.1 ± 1.4	23.8 ± 0.4
Toumboura I	T4	MG	3	–	3	0.98 ± 0.02	0 ± 0	48	–	–	42	14.9 ± 1.8	35.6 ± 0.9
	T5	MG	3	–	3	0.99 ± 0.04	4.6 ± 3.7	43	–	–	37	15.8 ± 2.0	37.0 ± 1.1
	T6	SG	300	None	16	0.89 ± 0.07	25.5 ± 6.2	2400	12	None	97	29.9 ± 3.1	37.1 ± 1.4
	T7	MG	3	–	3	0.98 ± 0.02	1.8 ± 4	48	–	–	42	22.2 ± 2.5	34.9 ± 1.2
Toumboura III	T14	SG	300	70	19	0.97 ± 0.02	4.5 ± 3.4	3900	30	40	314	32.7 ± 1.6	72.6 ± 1.5
	T15	SG	300	70	16	0.99 ± 0.04	10.5 ± 3.4	2400	20	40	221	33.6 ± 1.9	71.3 ± 1.8
	T16	SG	300	40	31	0.99 ± 0.02	7.7 ± 2.8	3800	24	30	395	33.2 ± 1.4	58.5 ± 1.1
Ravin de Missira	M1	SG	300	35	26	0.95 ± 0.02	4.2 ± 4.1	3900	22	35	311	31.7 ± 1.6	79.0 ± 1.6
	M2	SG	300	30	50	0.94 ± 0.01	7.6 ± 4.8	2500	22	40	126	30.8 ± 2.5	74.1 ± 2.3
	M3	SG	300	30	34	0.99 ± 0.02	5.4 ± 3.5	2400	20	30	239	34.6 ± 1.8	59.4 ± 1.4
Berges d'Alinguel	B3	SG	300	60	20	0.95 ± 0.05	20.1 ± 4.8	3900	40	80	84	27.4 ± 2.5	158.5 ± 4.9
	B4	SG	300	70	32	0.91 ± 0.03	11.7 ± 3.2	3400	41	70	145	41.8 ± 3.0	132.7 ± 5.2
	B5	SG	300	50	13	1.05 ± 0.03	28 ± 5.9	3900	45	50	84	42.3 ± 4.0	125.0 ± 6.5

Table 3
Summary of the dose rates (global errors, see Table 1), equivalent doses (statistical errors, see Table 2) and final age estimates (global error).

Site	Strat. unit	Sample	Total dose rate Gy/ka	CAM De (Gy)	Age (ka)
Fatandi V	?	F2	2.18 ± 0.15	22.8 ± 0.8	10.4 ± 0.9
		F5	2.41 ± 0.17	19 ± 0.5	7.9 ± 0.7
		F9	2.18 ± 0.25	23.8 ± 0.4	10.9 ± 0.9
Toumboura I	U_{CC}	T4	2.14 ± 0.29	35.6 ± 0.9	17 ± 1
		T5	3.12 ± 0.25	37 ± 1.1	17 ± 1
	U_G	T6	2.33 ± 0.26	37.15 ± 1.4	16 ± 1
		T7	2.36 ± 0.26	34.9 ± 1.4	15 ± 1
Toumboura III	U_J	T14	2.09 ± 0.15	72.6 ± 1.5	35 ± 3
		T15	2.16 ± 0.15	71.3 ± 1.8	33 ± 3
		T16	2.18 ± 0.16	58.5 ± 1.1	27 ± 2
Missira	U_B	M1	1.25 ± 0.17	79.0 ± 1.6	63 ± 5
		M2	1.06 ± 0.12	74.1 ± 2.2	70 ± 6
	U_J?	M3	1.91 ± 0.23	59.4 ± 1.4	31 ± 3
Berges d'Alinguel	C_{AG}	B3	1.79 ± 0.12	158.5 ± 4.9	88 ± 8
		B4	1.75 ± 0.12	132.7 ± 5.2	76 ± 7
		B5	1.85 ± 0.13	125.0 ± 6.5	67 ± 7

received high doses. For the others, removing such grains does not affect their dose recovery ratios (Fig. 7).

Single grain De measurements were systematically performed for high De samples (greater than 50 Gy). Single grain measurements were also performed for some of the youngest samples (F9, T6) in order to check that no additional problem such as bad bleaching or bio- turbation biased the multi-grain central De (see below). These different approaches (multi and single-grain) were performed on the same sam- ple (T6) in order to test if any intra-sample age variability occurred. For this sample at least, it was not the case: the single to multi-grain De ratio is consistent with unity at one sigma (0.98 ± 0.09).

For all these single grain measurements, we applied the D_0 selection criteria. Figs. 8 and 9 show that when the De central value is plotted as a function of the selected minimal D_0 value, the same pattern as the one observed for the dose recovery test is observed: discarding progressive- ly the grains having a small D_0 value leads to increase the central (CAM, Galbraith et al., 1999) De value until a plateau is reached when the pla- teau corresponds to high De values (here N 58 Gy), while there is no ini- tial rise when the plateau corresponds to low De values (here b 37 Gy). Inside this plateau, it can be considered that the choice of the threshold D_0 value does note influence the CAM De. Thus, for each sample that re- ceived a high dose, a D_0 threshold value was thus selected at the beginning of the CAM De plateau area in order to maximize the number of accepted grains. It is slightly different to the one determined from the dose recovery test. On the basis of the above, samples with no need for D0 thresholding were treated in multi grain mode (with the exception of T6 and F9, see previous paragraph).

In the previous section we have used the central age (actually dose) model of Galbraith et al. (1999). The pertinence of this choice however needs to be further discussed. Micromorphological observations have shown that quartz grains in B5 were coated with clay, which might have prevented good bleaching. However, its OD (42 ± 4%) is not signif- icantly different from that of B4 (42 ± 3%) where quartz grains were un- coated. Poor bleaching may have a priori also occurred because of the mode of transportation (fluvial or colluvial in many cases). However, Murray et al., 2012 have shown from the study of 67 modern fluvial samples that the mean offset to expect is 2 Gy, implying that only the youngest samples would be affected. In her review, Rittenour (2008) even suggests that only fluvial samples below 1 ka are significantly af- fected by poor bleaching phenomenon. As the central De values are N 19 Gy, and ages N 7 ka (see Section 5) and since no strong skewness is observed in the De distributions (Fig. 10 and Supplementary data), it seems reasonable to assume that poor bleaching did not significantly affect our samples.

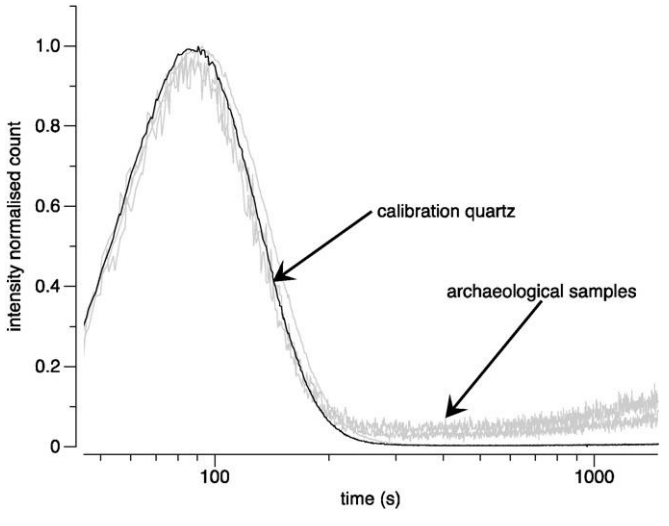

Fig. 4. Linearly modulated-OSL for 4 samples with De ranging from ca. 37 to 133 Gy, compared to the Risø calibration quartz. Natural signal is acquired during 2000 s while LED power is linearly increased from 0 to 70 mW/cm^2. The signal is dominated by the fast component and no evidence of middle or ultrafast components can be observed.

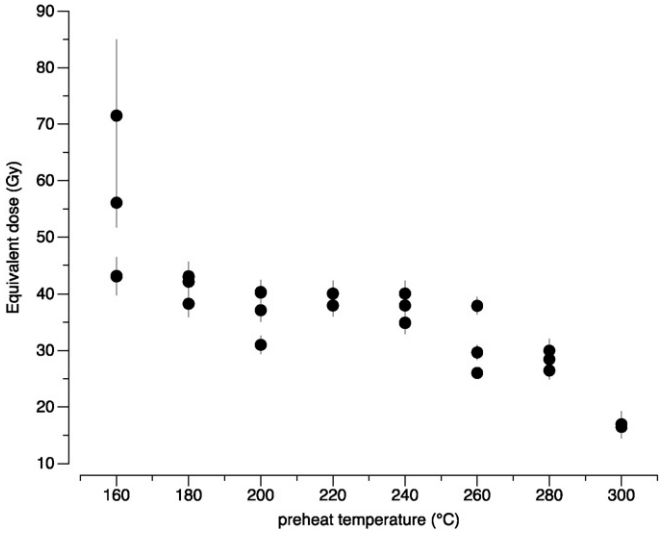

Fig. 5. Preheat temperature plateau for sample T5. Three multi-grains aliquots were measured for each temperature.

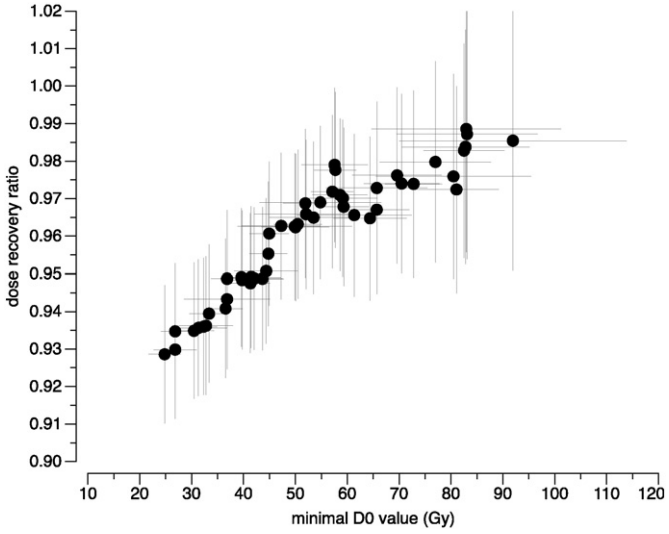

Fig. 6. Dose recovery ratio against minimal D_0 value of the grains used for the computation of the central recovered dose (Galbraith et al., 1999), sample T14, single-grain mode. The dose to recover was 70 Gy. It can be observed that for this sample, while the dose recovery ratio for the whole distribution is already within the [0.9;1.1] interval, it is significantly improved with D_0 thresholding.

Another reason for dose distribution enlargement could be the pres- ence of termites. Actually, macroscopic observations show that termite chambers are present in the sediments. While samples were taken as far as possible from those, further check is currently performed with micro- morphological inspections. In the meantime, to test for possible grain mixture, the Finite Mixture Model has been applied to all our samples. For both modes (2 and 3 components), all samples except one show that the vast majority of their grains (93% on average) fall within a sin- gle component; only sample T16 displays potentially two components (61%–39%), possibly indicating grain mixture problem. As a conse- quence, and without additional information, we have chosen to treat all our samples as not bioturbated. This choice recalls the one done by Tribolo et al. (2015) for their samples at Ounjougou: comparing central age and finite mixture models for 57 samples in somewhat similar kind of deposits, they found no significant difference in the final chronostratigraphy. However, we acknowledge there is no guaranty it is the same with the samples from the Falémé Valley.

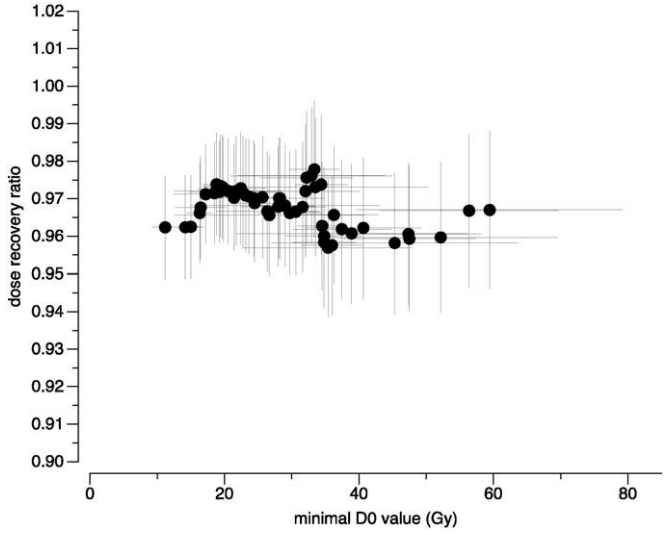

Fig. 7. Same graphic as Fig. 6 for a young sample (F2, dose to recover: 25 Gy), single-grain mode; considering uncertainty of the data, D_0 thresholding has no influence over the dose recovery ratio.

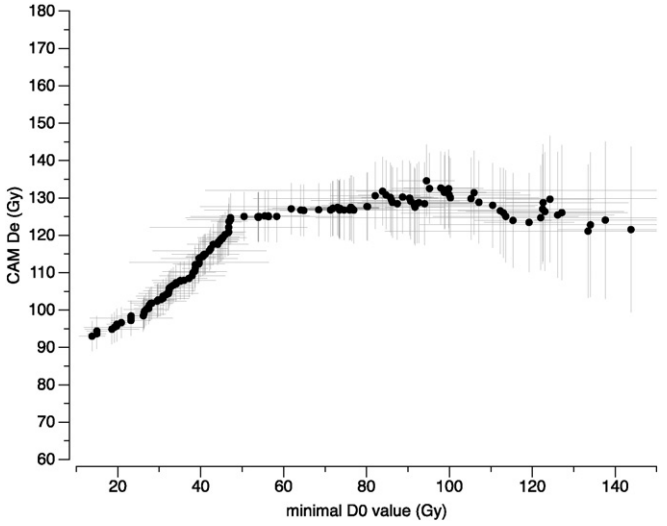

Fig. 8. Plot of CAM De over D_0 thresholding for a high De sample (B5), single-grain mode. For this sample, grains with D_0 value greater than 50 Gy tend to lower the CAM De.

Single grain OD values of our samples range between 27 and 42% and can be compared with those obtained for artificially bleached aliquots that were beta irradiated (OD values in single grain mode from 4 to 29%) and gamma irradiated (OD from 8 to 24%) for dose recovery tests. Assuming that the OD values observed for natural samples are not due to bioturbation or bleaching issues, this implies that the differ- ence of OD values between the natural and laboratory given dose is only caused by spatial dose rate heterogeneities (from 16 to 34%). Such OD values are not unlikely according to Guérin et al., (2015). In future works, this issue will be investigated with the help of beta autoradiogra- phy, modeling and computer simulations.

5. Ages and discussion

The ages given in Table 3 and Fig. 11 range from 88 ± 4 ka at the "Berges d'Alinguel" site to 7.9 ± 0.7 ka at Fatandi V.

At "Berges d'Alinguel",a *terminus ante quem* of 88 ± 8 ka is given for the lithic industry encountered in C_{AG} unit, indicating relatively old ages for these Lower to Early Middle Stone Age artifacts. This is consistent

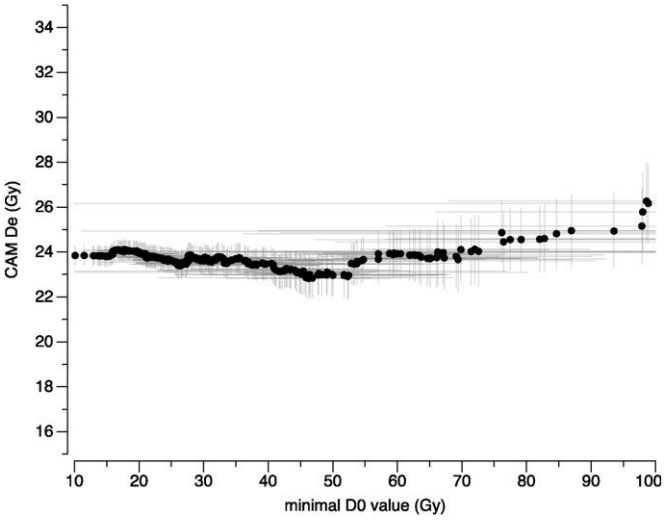

Fig. 9. Plot of CAM De over D_0 thresholding for a young sample (F9), single-grain mode. No significant influence of the D_0 value can be observed.

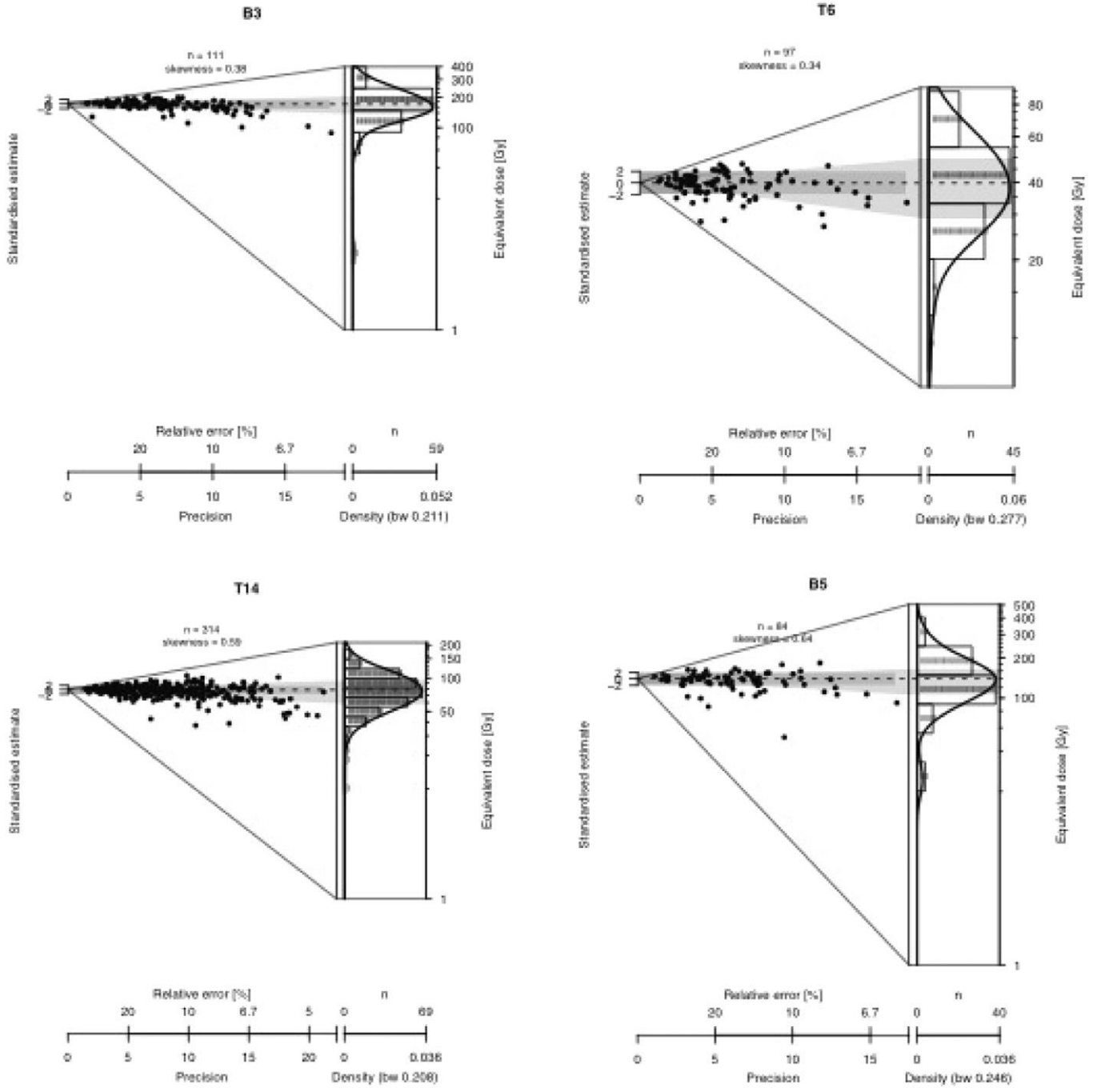

Fig. 10. Abanico plot (Dietze et al., 2016) of De distributions of samples T14, T6, B3 and B5.

with observations made at Ounjougou where a Levallois core with pref- erential removals was dated in the Late Middle Pleistocene (Soriano et al., 2010a, 2010b). In the "Ravin de Missira", samples M1 and M2 are located in the MIS4 while M3 takes place in the second half of the MIS 3. Considering the uncertainty of the numeric data, the apparent chrono-stratigraphic inversion between M1 (63 ± 5 ka) and M2 (70 ± 6 ka) is not significant. A *terminus ante quem* of 63 ± 5 ka is thus given for the MSA lithic artifact (bifacial rolled point in secondary position) of this site. The three samples taken at Toumboura III in the U_J unit are located in the second half of MIS 3 and the chrono-stratigraphic order is preserved. In particular, the archaeological level of this site is dated with sample T15 at 33 ± 3 ka. Chronological data ob- tained at Toumboura III (dominated by bifacial shaping) and to a lesser extent the "Ravin de Missira" (isolated bifacial point) correspond to the first reliable dates of Middle Stone Age bifacial shaping in the Falémé Valley. It is difficult to conclude with the current data whether this shap- ing technique was used continuously during MIS 3 or whether the oc- currences correspond to repetitions after periods of breaks. Meanwhile, this is reminiscent of alternation of that kind of industry during MIS 3 at Ounjougou (Soriano et al., 2010a, 2010b). Samples from Toumboura I range from 15 ± 1 to 17 ± 1 ka, in the middle of MIS 2. Sample T6 (16 ± 1 ka) matches within two sigma range with the calibrated radiocarbon age given by sample ETH-55080 (12,008 ± 176 2σ cal BCE; see Section 3). The archaeological unit of this site is dated in unit U_G by sample T7 at 15 ± 1 ka. Samples from Fatandi V range from 10.4 ± 0.9 to 7.9 ± 0.7 ka, dating the lithic industry of this site at the beginning of the Holocene. Therefore, the results for Fatandi V and Toumboura I highlight the presence of backed pieces at the

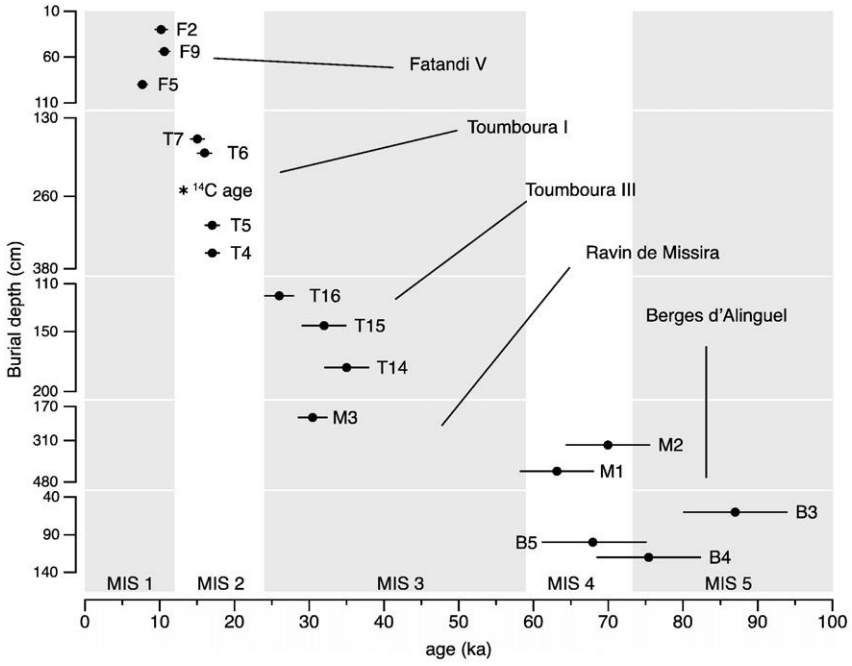

Fig. 11. Ages against their respective burial depth in each site, in centimeter from the actual ground surface. Details about the radiocarbon age can be found in Section 3. MIS boundaries are given after Martinson et al., 1987.

second half of the MIS 2 and onset of the Holocene and allow to discuss the issue of emergence of backing in Western Africa. These backed pieces can be microlithic (or not) segments and points. They are associ- ated with distinct production modes: simple debitage of small flakes and bladelets in Toumboura I, various debitages of wide bladelets in Fatandi V. Although backed pieces are present in both sites, differences in size, tool types, production and *chaîne opératoire* fragmentation are important: Toumboura I and Fatandi V sites then relate to two distinct expressions (Chevrier et al., in press).

Therefore, most of the last interglacial period is represented in the Falémé Valley, from the C_{AG} formation at the base of the stratigraphic sequence to U_{CC} and U_G at the top thereof. Since only a part of the sed- imentary units has been dated, no major stratigraphic gap can be distin- guished for now. Meanwhile, this shows that the geomorphological process of the Valley was favorable to the conservation of numerous for- mations. This is of primary importance for future archaeological and palaeoclimatic studies and we can expect to track palaeoclimatic oscilla- tions and events from the MIS 5 to the MIS 2 as in Ounjougou (Lespez et al., 2008). The record of layer within MIS 2 must also be highlighted. Here we have dated several (T4 to T7) samples within U_G and U_C at the end of MIS 2 and one (M3) at the second half of MIS 3. The presence of sedimentary units in between (C_{JS}, U_S) together with archaeological levels not presented here, offers thus a high potential for close inspec- tion of this poorly known time period.

In this paper, the first OSL dating results from the Falémé Valley were presented. Particular attention was paid to samples exhibiting high De values. A criteria based on the saturation level of the OSL signal has thus been used following recent recommendations by Thomsen et al. (2016), in order to discard the grains which were unable to prop- erly record the equivalent doses. As for the chronological results pre- sented here, two points must be highlighted: 1) the stratigraphic sequence of the Falémé Valley covers the vast majority of the Upper Pleistocene period and 2) MIS 2 seems to be particularly well preserved contrary to what has been observed at Ounjougou in particular (Huysecom, 2002; Huysecom et al., 2007; Lespez et al., 2008; Soriano et al., 2010a, 2010b; Rasse et al., 2012; Tribolo et al., 2015). Further dat- ing works will tend to confirm and specify the first chrono-cultural framework outlined here. However, the high potential and interest for both futures archaeological and palaeoenvironmental studies is already demonstrated. Undoubtedly, the stratigraphic sequence of the Falémé river offers the opportunity to bridge a gap in the palaeoenvironmental and human history in West Africa during the Late Quaternary period.

Acknowledgements

This study was supported by several sources of funding: The French Minister of National Education, Higher Education and Research (PhD scholarship of B. L.), the French Minister of Foreign Affairs (Mission Falémé, MAEDI, 2013-2016), the French National Research Agency and the Swiss National Science Foundation via the LaScArBx Labex (project number ANR-10-LABX-52), the SNF (project no. 101212-124657) and the joint project ANR-SNF 100019E-164071/ANR-15-CE33-0009-01,
the Faculty of Science of the University of Geneva, the SLSA Foundation for Swiss archaeological research abroad and the Institut Fondamental d'Afrique Noire (IFAN) at the University Cheikh Anta Diop of Dakar (UCAD). Thanks to the PACEA laboratory (UMR5199) for the laser dif- fraction analyses and to Queffelec A. in particular. We would like to thank our Senegalese and Malian collaborators, villagers and workers, for their invaluable help in the field.

Appendix A. Supplementary data

Supplementary data to this article can be found online at http://dx. doi.org/10.1016/j.jasrep.2016.05.001.

References

Bøtter-Jensen, L., Andersen, C.E., Duller, G.A.T., Murray, A.S., 2003. Developments in radi- ation, stimulation and observation facilities in luminescence measurements. Radiat. Meas. 37, 535–541.
Bøtter-Jensen, L., Bulur, E., Duller, G.A.T., Murray, A.S., 2000. Advances in luminescence in- strument systems. Radiat. Meas. 32, 523–528.
Camara, A., Duboscq, B., 1984. Le gisement préhistorique de Sansandé, basse vallée de la Falémé, Sénégal. Approche typologique et stratigraphique. l'Anthropologie 88 (3), 377–402.
Camara, A., Duboscq, B., 1987. Contexte chronostratigraphique des outillages du palélithique évolué dans l'est du Sénégal. l'Anthropologie 91 (2), 511–520.
Camara, A., Duboscq, B., 1990. La fouille d'un site acheuléen à Djita (basse vallée de la Falémé, Sénégal). l'Anthropologie 293–304.

Casey, J.L., Sawatzky, R., Godfrey-Smith, D., D'Andrea, A.C., Wollstonecroft, M., Hawkins, A., 1997. Report of investigations at the Birimi Site in Northern Ghana. Nyame Akuma 48, 32–38.

Chenorkian, R., 1983. Ivory Coast prehistory: recent developments. Afr. Archaeol. Rev. 1 (1), 127–142.

Chevrier, B., Huysecom, É., Soriano, S., Rasse, M., Lespez, L., Lebrun, B., Tribolo, C., submit- ted. Between continuity and discontinuity: an overview of the West African Paleolith- ic over the last 200,000 years. Quat. Int.

Chevrier, B., Rasse, M., Lespez, L., Tribolo, C., Hajdas, I., Guardiola Fígols, M., Lebrun, B., Leplongeon, A., Camara, A., Huysecom, É., in press. West African Palaeolithic history: New archaeological and chronostratigraphic data from the Falémé valley, astern Senegal. Quat. Int.

Cornelissen, E., 1996. Shum Laka (Cameroon): late Pleistocene and early Holocene de- posits. In: Pwiti, G., Soper, R. (Eds.), Aspects of African Archaeology. Congress of the Panafrican Assoc. for Prehistory and Related Studies, 10 (Harare, June 1995). Univ. of Zimbabwe Publ., Harare, pp. 257–263.

Cornelissen, E., 2003. On microlithic quartz industries at the end of the Pleistocene in Cen- tral Africa: the evidence from Shum Laka (NW Cameroon). Afr. Archaeol. Rev. 20, 1–24.

Dietze, M., Kreutzer, S., Burow, C., Fuchs, M.C., Fischer, M., Schmidt, C., 2016. The abanico plot: visualising chronometric data with individual standard errors. Quat. Geochronol. 31, 12–18.

Diop, A., 1980. Une nouvelle datation de l"Acheuléen en Afrique de l"Ouest. Annales de la Faculté des Lettres et Sciences Humaines. 10, pp. 283–291.

Duller, G.A.T., 2003. Distinguishing quartz and feldspar in single grain luminescence mea- surements. Radiat. Meas. 37 (2), 161–165.

Duller, G.A.T., 2015. The analyst software package for luminescence data: overview and recent improvements. Ancient TL 33 (1), 35–42.

Duller, G.A.T., Bøtter-Jensen, L., Kohsiek, P., Murray, A.S., 1999. A high sensitivity optically stimulated luminescence scanning system for measurement of single sand-sized grains. Radiat. Prot. Dosim. 84, 325–330.

Galbraith, R.F., Roberts, R.G., Laslett, G.M., Yoshida, H., Olley, J.M., 1999. Optical dating of single and multiple grains of quartz from jinmium rock shelter, northern Australia: part I, experimental design and statistical models*. Archaeometry 41 (2) pp 339–364. Garcea, E.A.A., 2012. Successes and failures of human dispersals from North Africa. Quat. Int. 270, 119–128.

Guérin, G., Frouin, M., Talamo, S., Aldeias, V., Bruxelles, L., Chiotti, H.L., Dibble, P., Goldberg, P., Hublin, J.-J., Jain, M., Lahaye, C., Madelaine, S., Maureille, B., McPherron, S.J.P., Mercier, N., Murray, A.S., Sandgathe, D., Steele, T.E., Thomsen, K.J., Turq, A., 2015. A multi-method luminescence dating of the Palaeolithic sequence of La Ferrassie based on new excavations adjacent to the La Ferrassie 1 and 2 skeletons. J. Archaeol. Sci. 58, 147–166.

Guérin, G., Mercier, N., 2011. Determining gamma dose rates by field gamma spectrosco- py in sedimentary media: results of Monte Carlo simulations. Radiat. Meas. 46 (2), 190–195.

Guérin, G., Mercier, N., Adamiec, G., 2011. Dose-rate conversion factors: update. Ancient TL 29 (1), 1–4.

Guérin, G., Mercier, N., Nathan, R., Adamied, G., Lefrais, Y., 2015. Modelling dose rate to single grains of quartz in well-sorted sand samples: the dispersion arising from the presence of potassium feldspars and implications for single grain OSL dating. Quater- nary Geochronology 27 (C) pp 52–65.

Hawkins, A., Casey, J.L., Godfrey-Smith, D., D'Andrea, A.C., 1996. A middle stone age com- ponent at the Birimi Site, northern region, Ghana. Nyame Akuma 46, 34–36.

Huysecom, É., 1987. Die archäologische Forschung in Westafrika, Materialien zur allgemeinen und vergleichenden Archäologie vol. 33. C.H. Beck, München, pp. 1–2. Huysecom, É., 2002. Palaeoenvironment and human population in West Africa: an inter- national research project in Mali. Antiquity 76 (292), 335–336.

Huysecom, É., Jeanbourquin, C., Mayor, A., Chevrier, B., Loukou, S., Canetti, M., Diallo, M., Bocoum, H., Guèye, N.S., Hajdas, I., Lespez, L., Rasse, M., 2013. Reconnaissance dans la vallée de la Falémé (Sénégal oriental): la 15ème année de recherches du pro- gramme international "Peuplement humain et paléoenvironnement en Afrique de l'Ouest". Jahresbericht SLSA 2012 Zürich et Vaduz: Fondation Suisse-Liechtenstein pour les recherches archéologiques à l'étranger, pp. 25–112.

Huysecom, É., Ozainne, S., Robion-Brunner, C., Mayor, A., Ballouche, A., Coulibaly, N., Guindo, N., Keita, D., Le Drezen, Y., Lespez, L., Neumann, K., Eichhorn, B., Rasse, M., Schaer, K., Selleger, C., Serneels, V., Soriano, S., Terrier, A., Tribolo, C., 2007. Peuplement humain et paléoenvironnement en Afrique de l'Ouest: résultats de la neuvième année de recherches. Zürich et Vaduz: Fondation Suisse-Liechtenstein pour les recherches archéologiques a l'étranger. Jahresbericht SLSA 2006. Zürich, Vaduz, pp. 41–122.

Lespez, L., Rasse, M., Le Drezen, Y., Tribolo, C., Huysecom, E., Ballouche, A., 2008. L'évolution hydrogémorphologique de la vallée du Yamé (Pays Dogon, Mali): signal climatique et hydrosystème continental en Afrique de l'Ouest entre 50 et 4 ka. Géomorphologie: relief, processus, environnement. vol. 3, pp. 169–185.

Lombard, M., 2012. Thinking through the middle stone age of sub-Saharan Africa. Quat. Int. 270, 140–155.

Maley, J., Roset, J.P., Servant, M., 1971. Nouveaux gisements préhistoriques au Niger orien- tal; localisation stratigraphique. Bulletin de liaison–ASEQUA 31, 9–18.

Marliac, A., 1973. Prospection archéologique au Cameroun. Cahiers ORSTOM. Sc. Hum. X. 1, 67–95.

Marliac, A., Gavaud, M., 1975. Premiers éléments d'une séquence paléolithique au Camer- oun septentrional. Bulletin de liaison - ASEQUA 46, 53–66.

Martinson, D.G., Imbrie, J., Moore, T.C., Shackleton, N.J., 1987. Age dating and the orbital theory of the ice ages: development of a high-resolution 0 to 300,000-year chronostratigraphy. Quat. Res. 27, 1–29.

Mcbrearty, S., Brooks, A.S., 2000. The revolution that wasn't: a new interpretation of the origin of modern human behavior. J. Hum. Evol. 39 (5), 453–563.

Mercier, N., Falguères, C., 2007. Field gamma dose-rate measurement with a NaI(Tl) de- tector: re-evaluation of the "threshold" technique. Ancient TL 25, 1–4.

Michel, P., 1973. Les bassins des fleuves Sénégal et Gambie. Etude géomorphologique. Thèse Strasbourg, Mémoire ORSTOM. vol. 63 p. 750.

Mie, G., 1908. Beiträge zur Optik trüber Medien, speziell kolloidaler Metallösungen. Annalen der Physik, Leipzig 25, 377–445.

Murray, A.S., Thomsen, K.J., Masuda, M., Buylaert, J.P., Jain, M., 2012. Identifying well- bleached quartz using the different bleaching rates of quartz and feldspar lumines- cence signals. Radiat. Meas. 47, 688–695.

Murray, A.S., Wintle, A.G., 2000. Luminescence dating of quartz using an improved single- aliquot regenerative-dose protocol. Radiat. Meas. 32, 57–73.

Nelson, M.S., Rittenour, T.M., 2015. Using grain-size characteristics to model soil water con- tent: application to dose-rate calculation for luminescence dating. Radiat. Meas. 1–44. Prescott, J.R., Hutton, J.T., 1994. Cosmic ray contributions to dose rates for luminescence and ESR dating: large depths and long-term time variations. Radiat. Meas. 23 (2–3), 497–500.

Quickert, N.A., Godfrey-Smith, D.I., Casey, J.L., 2003. Optical and thermoluminescence dat- ing of middle stone age and Kintampo bearing sediments at Birimi, a multi- component archaeological site in Ghana. Quat. Sci. Rev. 22, 1291–1297.

Rasse, M., Tribolo, C., Soriano, S., Huysecom, É., 2012. Premières données chronostratigraphiques sur les formations pléistocènes de la «falaise» de Bandiagara (Mali, Afrique de l'Ouest). Quaternaire 23 (1), 5–23.

Reimer, P., Bard, E., Bayliss, A., Beck, J., Blackwell, P., Bronk Ramsey, C., Buck, C., Cheng, H., Edwards, R., Friedrich, M., Grootes, P., Guilderson, T., Haflidason, H., Hajdas, I., Hatté, C., Heaton, T., Hoffmann, D., Hogg, A., Hughen, K., Kaiser, K., Kromer, B., Manning, S., Niu, M., Reimer, R., Richards, D., Scott, E., Southon, J., Staff, R., Turney, C., Van Der Plicht, J., 2013. IntCal13 and Marine13 radiocarbon age calibration curves 0- 50,000 years cal BP. Radiocarbon 55 (4), 1869–1887.

Richter, D., Richter, A., Dornich, K., 2013. Lexsyg a new system for luminescence research. Geochronometria 40 (4), 220–228.

Rittenour, T.M., 2008. Luminescence dating of fluvial deposits: applications to geomor- phic, palaeoseismic and archaeological research. Boreas 37, 613–635.

Shaw, T., Daniels, S.G.H., 1984. Excavations at Iwo Eleru, Ondo State, Nigeria. West Afr. J. Archaeol. 14 269 p.

Soriano, S., Rasse, M., Tribolo, C., Huysecom, E., 2010a. In: Allsworth-Jones, P. (Ed.), "Ounjougou: A Long Middle Stone Age Sequence in the Dogon Country (Mali)" in West African Archaeology: New Developments, New Perspectives. Archaeopress, Ox- ford, pp. 1–14.

Soriano, S., Rasse, M., Tribolo, C., Huysecom, É., 2010b. Ounjougou (Pays dogon, Mali): une séquence à haute résolution pour le Paléolithique moyen d'Afrique sahélienne. Afrique Archéologie Arts 6, 1–18.

Thomsen, K.J., Murray, A.S., Buylaert, J.P., Jain, M., Hansen, J.H., Aubry, T., 2016. Testing sin- gle-grain quartz OSL methods using sediment samples with independent age control from the Bordes-Fitte rockshelter (Roches d'Abilly site, Central France). Quaternary Geochronology 31 (C), pp 77–96.

Tribolo, C.S., Rasse, M., Soriano, S., Huysecom, É., 2015. Defining a chronological frame- work for the middle stone age in West Africa: comparison of methods and models for OSL ages at Ounjougou (Mali). Quat. Geochronol. 29, 80–96.

Wintle, A.G., Murray, A.S., 2006. A review of quartz optically stimulated luminescence characteristics and their relevance in single-aliquot regeneration dating protocols. Radiat. Meas. 41 (4), 369–391.